Check for updates

Received: 15 September 2022 | Revised: 2 January 2023 | Accepted: 14 February 2023 | Published on: 24 May 2023

DOI: 10.1002/qj.4476

Quarterly Journal of the Royal Meteorological Society

RESEARCH ARTICLE

On a new one-dimensional k–ε turbulence closure for building-induced drag

Andrea Zonato[1] | **Alberto Martilli**[2] | **Jose Luis Santiago**[2] | **Dino Zardi**[1] | **Lorenzo Giovannini**[1]

[1]Atmospheric Physics Group, Department of Civil, Environmental and Mechanical Engineering, University of Trento, Trento, Italy

[2]Center for Energy, Environment and Technology (CIEMAT), Madrid, Spain

Correspondence
Andrea Zonato, Atmospheric Physics Group, Department of Civil, Environmental and Mechanical Engineering, University of Trento, Trento, Italy.
Email: andrea.zonato@unitn.it

Abstract

Various urban canopy parameterizations (UCPs) have been developed in the last two decades to take into account the modifications induced by buildings on mean flow and turbulent fields in mesoscale meteorological models, the typical spatial resolution of which cannot resolve urban structures explicitly. In particular, several multilayer UCPs have been proposed, successfully reproducing wind-flow characteristics in the urban environment. However, they often rely on length scales for the calculation of the eddy viscosity and the dissipation rate, which need to be tuned for various urban configurations. The main objective of this work is to address this shortcoming, by developing a new one-dimensional turbulence closure that takes building-induced turbulence into account independently of turbulence length scales. This model directly solves not only the equation for turbulent kinetic energy but also the equation for its dissipation rate (k–ε model). Similar closure schemes have been successfully adopted for vegetated canopies, but their applicability to urban canopies is still unknown. The performance of the new k–ε model, with additional sources and sinks for wind speed, turbulent kinetic energy, and dissipation rate, is tested by means of single-column simulations in idealized urban areas, using different building packing densities. Results are in good agreement with spatially averaged building-resolving CFD simulations. In particular, vertical profiles of mean and turbulent variables show better results with respect to simulations using turbulence closures adopting a parameterization of turbulence length scales. The best improvements are obtained for wind speed, reducing errors to half the typical values for standard UCP for high packing densities, and for the dissipation rate. Furthermore, besides the enhancement in the reproduction of the mean flow for urban areas, the proposed turbulence closure does not need additional tuning of coefficients depending on the packing density, resulting in a more general and efficient scheme.

KEYWORDS

building-induced turbulence, CFD, k–ε, RANS, turbulence modeling

Abbreviations: CFD, computational fluid dynamics; DNS, direct numerical simulations; LES, large-eddy simulations; MOST, Monin–Obukhov similarity theory; PBL, planetary boundary layer; RANS, Reynolds-averaged Navier–Stokes; RMSE, root-mean-square error; TKE, turbulent kinetic energy; UCL, urban canopy layer; UCPs, urban canopy parameterizations.

This is an open access article under the terms of the Creative Commons Attribution-NonCommercial-NoDerivs License, which permits use and distribution in any medium, provided the original work is properly cited, the use is non-commercial and no modifications or adaptations are made.
© 2023 The Authors. *Quarterly Journal of the Royal Meteorological Society* published by John Wiley & Sons Ltd on behalf of the Royal Meteorological Society.

1 | INTRODUCTION

Accurate mesoscale meteorological modeling in urban areas is critical for assessing urban climate and informing air quality and urban planning studies. However, the main challenges in simulating atmospheric processes within the urban canopy layer (UCL) arise from the heterogeneity of the urban land use. The horizontal spatial resolution of mesoscale models, usually set to ∼ 1 km for computational reasons, cannot resolve turbulent structures and atmospheric flows around buildings explicitly. Appropriate urban canopy parameterizations (UCPs), consistent with turbulence schemes present in state-of-the-art numerical weather prediction models, are required to consider the effect of urban obstacles and surfaces. Roth (2000) highlighted that the two main effects induced by urban structures on atmospheric processes in the planetary boundary layer (PBL) are associated with the mechanical drag from buildings and the heating of urban surfaces, which modifies the vertical thermal structure. In the past decades, UCPs have been developed to model the interaction between urban structures and the airflow within mesoscale models, at different levels of complexity. The simplest way to model urban obstacles within numerical models is to increase the roughness length and modify soil thermal properties in the context of the Monin–Obukhov similarity theory (MOST). With a more advanced approach, in single-layer UCPs the UCL is represented in the first vertical level of the atmospheric model, and the effects of the built environment are represented by means of infinitely long urban canyons, presenting geometrical characteristics based on average urban morphology features (Masson, 2000; Kusaka *et al.*, 2001; Kanda *et al.*, 2005; Giovannini *et al.*, 2013). Increasing the complexity, in multilayer schemes the UCP interacts with several levels of the atmospheric model, treating urban areas as a porous medium where the sink of momentum depends on the drag induced by buildings (Martilli *et al.*, 2002; Coceal *et al.*, 2006; Di Sabatino *et al.*, 2008; Masson and Seity, 2009). The latter is usually proportional to the square of the mean wind speed perpendicular to the building surface times a sectional drag coefficient (C_d), which is generally set constant with height and building packing density, assuming values from 0.1 (Uno *et al.*, 1989) to 1 (Coceal and Belcher, 2004). However, observational studies and microscale models demonstrate that C_d depends on the city configuration and the height from the ground (Santiago *et al.*, 2008; Ahmad Zaki *et al.*, 2012; Chen *et al.*, 2017). Regarding the turbulent closure, UCPs generally use first-order K closures based on a mixing length scale, or 1.5-order closures based on a prognostic equation for turbulent kinetic energy, but are generally dependent on a semi-empirical turbulent length scale (k–ℓ models).

A straightforward comparison of the output from UCPs with data from point measurements is usually not feasible, since the simulated flow is representative of spatial averages over mesoscale grid points. For this reason, Santiago and Martilli (2010) proposed to use microscale computational fluid dynamics (CFD) models, based on Reynolds-averaged Navier–Stokes (RANS) equations, to validate and develop UCPs. More recently, Nazarian *et al.* (2020) proposed a similar method but based on the validation of UCPs with large-eddy simulations (LES). Microscale models, based on either RANS or LES approaches, have a resolution high enough to resolve the urban structures explicitly, and therefore even the turbulent flows around buildings. Examples of such simulations can be found in Santiago *et al.* (2008); Antoniou *et al.* (2017); Giometto *et al.* (2017); Dai *et al.* (2018); Nazarian *et al.* (2020); Auvinen *et al.* (2020). Outputs of building-resolving microscale simulations need to be spatially averaged, to inform and improve one-dimensional mesoscale UCPs. Adopting this method, Santiago and Martilli (2010) used CFD simulations over staggered arrays of cubes, validated against direct numerical simulations (DNS) and wind-tunnel data (Santiago *et al.*, 2008), to upgrade the multilayer UCP presented in Martilli *et al.* (2002), based on a 1.5-order k–ℓ turbulence closure. Specifically, CFD outputs have been used to evaluate the dependence of the mixing length scale, the dissipation rate l_ε, and the drag coefficient C_d on packing density and height from the ground. Subsequently, Nazarian *et al.* (2020) improved this UCP further, using LES to estimate the dependence of the displacement height and turbulent length scale l_k on building packing density, through the tuning of related coefficients.

Models adopting a k–ℓ-based turbulence closure require an empirical or semi-empirical computation of the turbulence length scales, which are often specifically adapted for particular case studies. Moreover, even in the case of flat and heterogeneous surfaces, the estimation of the length scale relies on empirical data and physical approximations. To overcome the above shortcomings, we propose a multilayer UCP, built on the same model setup as Santiago and Martilli (2010) and Nazarian *et al.* (2020), which does not depend on a k–ℓ turbulence closure. Rather, the turbulent transport is modeled with a k–ε approach. Indeed, k–ε based turbulence closures differ from k–ℓ closures by the additional prognostic equation of the dissipation rate of turbulent kinetic energy ε. This turbulent closure, first adopted for atmospheric flows by Launder and Spalding (1974), was employed successfully in the following years for various PBL schemes

1477870x, 2023, 754, Downloaded from https://rmets.onlinelibrary.wiley.com/doi/10.1002/qj.4476 by Universita Di Trento, Wiley Online Library on [27/09/2023]. See the Terms and Conditions (https://onlinelibrary.wiley.com/terms-and-conditions) on Wiley Online Library for rules of use; OA articles are governed by the applicable Creative Commons License

(Duynkerke, 1988; Langland and Liou, 1996; van der Laan *et al.*, 2017; Zeng *et al.*, 2020; Zhang *et al.*, 2020), and more recently by Zonato *et al.* (2022). Beljaars *et al.* (1987) compared k–ℓ and k–ε schemes and found that the k–ε approach retains memory effects better in velocity scales when surface conditions change. Memory effects are only considered when a prognostic equation is included, since the dissipation rate depends on its distribution at the previous time step, including its vertical transport. This kind of closure was also employed for multilayer vegetation canopy models (Wilson *et al.*, 1998; Sanz, 2003; Katul *et al.*, 2004; Tolladay and Chemel, 2021), but never before in the case of urban canopies. In this work, we propose two different UCPs, differing in the expressions for the additional sources/sinks due to buildings in the prognostic equations of the turbulent kinetic energy and its dissipation rate. The aim is to develop a suitable UCP with state-of-the-art turbulence closures, eventually to be embedded within NWP models. The same spatially averaged CFD simulations adopted in Santiago and Martilli (2010) are used as guidance to set the values of an additional drag coefficient for the prognostic equation of the dissipation rate and to validate the k–ε based urban canopy parameterizations.

The article is organized as follows: Section 2 describes the dynamical part of the urban canopy parameterization, along with the turbulence closure tested in this work. The setup of the one-dimensional mesoscale (UCP) and three-dimensional microscale (CFD) simulations is described in Section 3. Section 2.1 presents the additional novel terms in the prognostic equations to account for the drag induced by buildings, while results for configurations with different packing densities are shown in Section 4. Finally, conclusions are given in Section 5.

2 | MODEL DESCRIPTION

The momentum equation solved by a mesoscale model over urban areas involves two averaging processes: in time (or ensemble), to filter out turbulent motions, and in space over the grid cell, to filter out the subgrid structures, the characteristic length scales of which are smaller than the grid resolution (Santiago and Martilli, 2010). Applying both averages, and assuming horizontal homogeneity and no mean vertical motion, the equation for the horizontal wind speed u reads

$$\frac{\partial \rho \langle \overline{u} \rangle}{\partial t} = -\frac{\partial \rho \langle \overline{u'w'} \rangle}{\partial z} - \frac{\partial \rho \langle \tilde{u}\tilde{w} \rangle}{\partial z} - \rho D_u, \tag{1}$$

where the overbars refer to the time (or ensemble) mean, angle brackets to the space average, u' and w' represent the deviation of the instantaneous velocities from the time-averaged value at the same point (turbulent fluctuation), $\tilde{u}$ and $\tilde{w}$ are the departure of the mean wind component from its spatial average (dispersive fluctuation), and ρ is the air density, assumed to be constant with height. The first term on the right-hand side is the contribution of the turbulent momentum flux, the second represents the dispersive flux, and the latter (D_u) the drag induced by buildings, which will be explained in Section 2.1. In this work, we neglect the contribution of the dispersive flux, as done in Santiago and Martilli (2010) and Nazarian *et al.* (2020). This will result in a limitation for the present model. The spatially averaged turbulent momentum flux is parameterized through the K theory:

$$\langle \overline{u'w'} \rangle = -K_m \frac{\partial \langle \overline{u} \rangle}{\partial z}, \tag{2}$$

where K_m is the eddy viscosity. In Santiago and Martilli (2010), K_m is calculated using a k–ℓ closure (as in Martilli *et al.* (2002), based on Bougeault and Lacarrere (1989)):

$$k_m = C_k \ell_k \langle \overline{k} \rangle^{1\backslash 2}, \tag{3}$$

where C_k is a model constant, ℓ_k is the turbulent length scale and $\langle \overline{k} \rangle$ the spatially and temporally averaged turbulent kinetic energy (TKE). A detailed description of the closure constants and length scales for this parameterization is shown in Section 2.1. On the other hand, in the k–ε scheme, since we aim to avoid the definition of an ad hoc length scale, the diffusion coefficient is computed as

$$K_m = C_\mu \frac{\langle \overline{k} \rangle^2}{\langle \overline{\varepsilon} \rangle}, \tag{4}$$

where C_μ is a model constant, set to 0.09 (Launder and Spalding, 1983), and ε is the spatially and temporally averaged TKE dissipation rate. The spatially and temporally averaged TKE is calculated through its prognostic equation, considering horizontal homogeneity and neglecting pressure fluctuations:

$$\frac{\partial \rho \langle \overline{k} \rangle}{\partial t} = \frac{\partial}{\partial z}\left(\rho K_m \frac{\partial \langle \overline{k} \rangle}{\partial z}\right) + \rho K_m \left[\left(\frac{\partial \langle \overline{u} \rangle}{\partial z}\right)^2 + \left(\frac{\partial \langle \overline{v} \rangle}{\partial z}\right)^2\right] - \rho K_m \frac{g}{\theta_0}\frac{\partial \langle \overline{\theta} \rangle}{\partial z} - \rho \langle \overline{\varepsilon} \rangle + \rho D_k, \tag{5}$$

where the first term on the right-hand side is the vertical diffusion of TKE, the second the production by shear, the third the production/destruction by buoyancy, the fourth the TKE dissipation, and D_k is the source of $\langle \overline{k} \rangle$ generated by the interaction between the buildings and the mean flow. In this particular case, where we assume neutral

1477870x, 2023, 754, Downloaded from https://rmets.onlinelibrary.wiley.com/doi/10.1002/qj.4476 by Universita Di Trento, Wiley Online Library on [27/09/2023]. See the Terms and Conditions (https://onlinelibrary.wiley.com/terms-and-conditions) on Wiley Online Library for rules of use; OA articles are governed by the applicable Creative Commons License

stratification, the buoyant production term is zero. In this equation, $\langle\overline{\varepsilon}\rangle$ needs to be evaluated. Assuming a k–ℓ closure, Santiago and Martilli (2010) use the following diagnostic equation:

$$\langle\overline{\varepsilon}\rangle = C_\varepsilon \frac{\langle\overline{k}\rangle^{3\backslash 2}}{l_\varepsilon}, \tag{6}$$

where the length scale l_ε is required to obtain $\langle\overline{\varepsilon}\rangle$. In order to avoid defining a length scale as in Equation 6, in the k–ε approach $\langle\overline{\varepsilon}\rangle$ is calculated through its prognostic equation, similarly to Katul *et al.* (2004):

$$\begin{aligned}\frac{\partial\rho\langle\overline{\varepsilon}\rangle}{\partial t} = &-\frac{\partial}{\partial z}\left(\frac{1}{\sigma_\varepsilon}\rho K_m\frac{\partial\langle\overline{\varepsilon}\rangle}{\partial z}\right)\\ &+\rho K_m\left(c_1\left[\left(\frac{\partial\langle\overline{u}\rangle}{\partial z}\right)^2+\left(\frac{\partial\langle\overline{v}\rangle}{\partial z}\right)^2\right]\right.\\ &\left.-c_3\frac{g}{\theta_0}\frac{\partial\langle\overline{\theta}\rangle}{\partial z}\right)\frac{\langle\overline{\varepsilon}\rangle}{\langle\overline{k}\rangle}-c_2\frac{\langle\overline{\varepsilon}\rangle^2}{\langle\overline{k}\rangle}+\rho D_\varepsilon,\end{aligned} \tag{7}$$

where the first term on the right-hand side is the vertical diffusion, the second term is the production/destruction of dissipation rate by shear (first part) and buoyancy (second part), the third is the dissipation, and the fourth (D_ε) is the source of $\langle\overline{\varepsilon}\rangle$ generated by the interaction between the buildings and the mean flow. σ_ε, c_1, c_2, and c_3 are model constants, usually set to 1.3, 1.44, 1.92, and 1.44 (Launder and Spalding, 1983).

2.1 | Drag induced by buildings

Multilayer UCPs treat urban areas as a porous material, modeled by means of a drag force (see Equations 10–12). The latter needs to be parameterized, as buildings cannot be resolved explicitly because the resolution of mesoscale models is usually much larger than the building dimension. The common model for D_u, the physical meaning of which is an extra negative horizontal pressure gradient induced by the buildings, makes the sink of momentum associated with the canopy obstacles dependent on the wind speed itself. At a certain height z, the drag term for wind speed reads

$$D_u = \frac{1}{\rho}\left\langle\frac{\partial\overline{p}}{\partial x}\right\rangle\Big|_z = -S(z)\,C_\mathrm{d}\langle\overline{u(z)}\rangle\left|\langle\overline{u(z)}\rangle\right|, \tag{8}$$

where $S(z)$ is the upwind vertical surface building density, C_d is the sectional drag coefficient (to be modeled), and $\langle\overline{u(z)}\rangle$ is the spatially averaged mean wind speed at level z.

The drag term for TKE is parameterized, in analogy with D_u, as

$$D_k = S(z)\,C_\mathrm{d}\left|\langle\overline{u(z)}\rangle\right|^3. \tag{9}$$

A turbulence closure with no prognostic equations for the dissipation rate (k–ℓ hereafter) does not need any additional term, and for this reason it has been widely used in literature.

On the other hand, one of the primary reasons discouraging the development of k–ε models for canopy-layer flows is the difficulty in modeling the effects of the canopy (Katul *et al.*, 2004). Indeed, besides parameterizing the terms D_u and D_k, D_ε also has to be modeled, and modeling D_ε is the primary weakness of a k–ε approach (Wilson *et al.*, 1998).

In the literature, no examples are found using k–ε closures in UCPs. For vegetated canopies, however, different approaches have been developed. The simplest one is the closure adopted by Tolladay and Chemel (2021), where the dissipation rate is increased by a factor depending linearly on the wind speed and on $\langle\overline{\varepsilon}\rangle$ itself:

$$D_\varepsilon = S(z)\,C_{\mathrm{d}\varepsilon}|\langle\overline{u}\rangle|\langle\overline{\varepsilon}\rangle, \tag{10}$$

where $C_{\mathrm{d}\varepsilon}$ is the drag coefficient for the dissipation rate. This closure will be called k–ε–$1T$ hereafter, since it depends on a single additional term ($C_{\mathrm{d}\varepsilon}$) with respect to Santiago and Martilli (2010).

Moving towards more complex models, and exploiting the analogy with parameterizations for vegetated canopies, Sanz (2003) and Katul *et al.* (2004) suggested the following formulations for D_k and D_ε, respectively:

$$D_k = S(z)\,C_\mathrm{d}\left(\alpha_1|\langle\overline{u}\rangle|^3-\alpha_2|\langle\overline{u}\rangle|\langle\overline{\varepsilon}\rangle\right), \tag{11}$$

$$D_\varepsilon = S(z)\,C_\mathrm{d}\left(\beta_1\frac{\langle\overline{\varepsilon}\rangle}{\langle\overline{k}\rangle}|\langle\overline{u}\rangle|^3-\beta_2|\langle\overline{u}\rangle|\langle\overline{\varepsilon}\rangle\right), \tag{12}$$

where C_d is the drag coefficient of Equation 8 and α_1, α_2, β_1, and β_2 are closure constants to be determined. The first terms on the right-hand side are based on the standard dimensional analysis of the k–ε approach. The second term comes from wind-tunnel studies (Liu *et al.*, 1996): it was introduced to fit experimental data. Its physical meaning is that obstacles lead to a "short-circuiting" of Kolmogorov's cascade (Poggi *et al.*, 2004). This closure is called k–ε–$3T$ hereafter since three additional terms have been added (and modeled) with respect to Santiago and Martilli (2010). Those terms are the second part on the right-hand side of Equation 11 and the right-hand side of Equation 12.

In the next subsection (Section 2.2), we will present the models developed to parameterize C_d (appearing in Equations 8,9,11, and 12), $C_{\mathrm{d}\varepsilon}$, used to calculate the drag term for $\langle\overline{\varepsilon}\rangle$ in Equation 10, and the four coefficients in Equations 11 and 12.

1477870x, 2023, 754, Downloaded from https://rmets.onlinelibrary.wiley.com/doi/10.1002/qj.4476 by Universita Di Trento, Wiley Online Library on [27/09/2023]. See the Terms and Conditions (https://onlinelibrary.wiley.com/terms-and-conditions) on Wiley Online Library for rules of use; OA articles are governed by the applicable Creative Commons License

2.2 | The drag coefficient

The drag coefficients C_d and $C_{d\varepsilon}$ need to be parameterized for various urban configurations. Usually, C_d is set constant with plan area ratio and height, with values ranging from 0.1–1 (Coceal and Belcher, 2004). However, experiments have shown that it depends on the plan area ratio and on the building horizontal distribution (staggered or aligned), and it has a strong dependence on height (Santiago *et al.*, 2008). Suitable information about the vertical profiles of C_d and $C_{d\varepsilon}$ is not easily obtained through wind-tunnel experiments, because it is difficult to quantify the pressure deficit for an obstacle, and the drag coefficient close to the ground is usually very large because of low wind speeds and not integrable within one-dimensional models. Accordingly, Santiago and Martilli (2010) calculated an equivalent drag coefficient for staggered buildings distribution, constant with height, that appears in the drag force for TKE and u. This calculation involves the pressure differences between the two sides of a building, obtained through a building-resolving RANS-CFD simulation, spatially averaged over the simulation domain:

$$C_{deq} = \frac{\frac{-1}{\rho h}\int_0^h \Delta\langle\overline{p(z)}\rangle dz}{\frac{-1}{h}\int_0^h \langle\overline{u(z)}\rangle\left|\langle\overline{u(z)}\rangle\right| dz}. \tag{13}$$

The drag coefficient computed by this method, hereafter called C_{deq}, depends on the configuration (staggered or aligned buildings) and on the plan area ratio. By fitting the results of CFD simulations performed with different plan area ratios, Santiago and Martilli (2010) found the following relation between C_{deq} and λ_p for staggered building arrays:

$$C_{deq}(\lambda_p) = \begin{cases} 3.31\ \lambda_p^{0.47} & \text{if } \lambda_p \le 0.29, \\ 1.85 & \text{if } \lambda_p > 0.29. \end{cases} \tag{14}$$

The variation of C_{deq} with λ_p is shown in Figure 1a. As expected, the drag coefficient increases with increasing λ_p. However, once the threshold of $\lambda_p = 0.29$ is reached, the flow interprets the top of the building array as a displaced surface and the drag coefficient maintains a constant value.

The k–ℓ closure also requires a model for the length scales l_k and l_ε. The following relation between these two length scales can be obtained using Equations 3,4, and 6:

$$C_k \ell_k = C_\mu \frac{\ell_\varepsilon}{C_\varepsilon}. \tag{15}$$

Therefore, from the CFD outputs, using Equation 6, Santiago and Martilli (2010) calculated the ratio $\ell_\varepsilon/C_\varepsilon$, assuming this value to be constant within the canopy layer ($z/h < 1$) and increasing linearly above the canopy layer, changing slope at $z/h = 1.5$:

$$\frac{\ell_\varepsilon}{C_\varepsilon} = \begin{cases} a_1\,(h-d) & \text{if } z/h \le 1, \\ a_1\,(z-d) & \text{if } 1 < z/h \le 1.5, \\ a_2\,(z-d_2) & \text{if } z/h > 1.5, \end{cases} \tag{16}$$

where $a_1 = 2.24$ and $a_2 = 1.12$ are calculated using the urban configuration with $\lambda_p = 0.25$, d_2 is computed in order to make $\ell_\varepsilon/C_\varepsilon$ continuous at $z/h = 1.5$, and $d/h = \lambda_p^{0.13}$, with d the displacement height, obtained by fitting the CFD data in the different configurations.

The advantage of using a k–ε turbulence scheme for this particular case is that a length scale is not needed. Therefore the calculation of the different length scales and the displacement height d is not required. $C_{d\varepsilon}$ needs to be calculated for the k–ε–$1T$ closure, while the k–ε–$3T$ scheme adopts the same drag coefficient as the k–ℓ closure. However, despite attempts to obtain $C_{d\varepsilon}$ by inverting Equations 22 and 10 and fitting the results, we could not find reasonable values, since within the canopy the flow variables tend to reach very small (e.g., u) or too large values (like $\langle\overline{\varepsilon}\rangle$). For this reason, for each packing density, a large number of simulations was performed varying $C_{d\varepsilon}$, and taking the value that minimizes the average root-mean-square error (RMSE) of u, k, and ε along the vertical 1-D domain, adopting the CFD output as the reference. The dependence of $C_{d\varepsilon}$ on λ_p (shown in Figure 1) follows two different functions: a parabola up to $\lambda_p = 0.25$ and a straight line for higher values. Its dependence on λ_p reads

$$C_{d\varepsilon}\left(\lambda_p\right) = \begin{cases} a_1\lambda_p^{-b_1} + b_2 & \text{if } \lambda_p \le 0.25, \\ -a_2\lambda_p + b_3 & \text{if } \lambda_p > 0.25, \end{cases} \tag{17}$$

with $a_1 = 0.07$, $b_1 = -1.4$, $b_2 = 8.3$, $a_2 = 14.8$, and $b_3 = 12.4$. Note that, while C_d increases with increasing λ_p, $C_{d\varepsilon}$ decreases with increasing λ_p. The reason is that large values of λ_p tend to decrease the turbulence generated within the canopy layer, and a decrease in turbulence intensity is reflected in a decrease in the dissipation rate $\langle\overline{\varepsilon}\rangle$. As we will show in Section 4, for large values of λ_p the flow variables are almost null within the canopy layer and the horizontal flow starts to develop above the roof level.

The limitation of the model using $C_{d\varepsilon}$ estimated with the CFD output lies in the function for the drag coefficient for $\lambda_p < 0.25$. With λ_p approaching zero, $C_{d\varepsilon}$ tends to increase rapidly, and, proportionally, so does the dissipation rate. Therefore, additional CFD simulations should be performed to estimate the drag coefficient for $\lambda_p < 0.0625$, where this model is not able to reproduce the flow correctly in the UCL.

1477870x, 2023, 754, Downloaded from https://rmets.onlinelibrary.wiley.com/doi/10.1002/qj.4476 by Universita Di Trento, Wiley Online Library on [27/09/2023]. See the Terms and Conditions (https://onlinelibrary.wiley.com/terms-and-conditions) on Wiley Online Library for rules of use; OA articles are governed by the applicable Creative Commons License

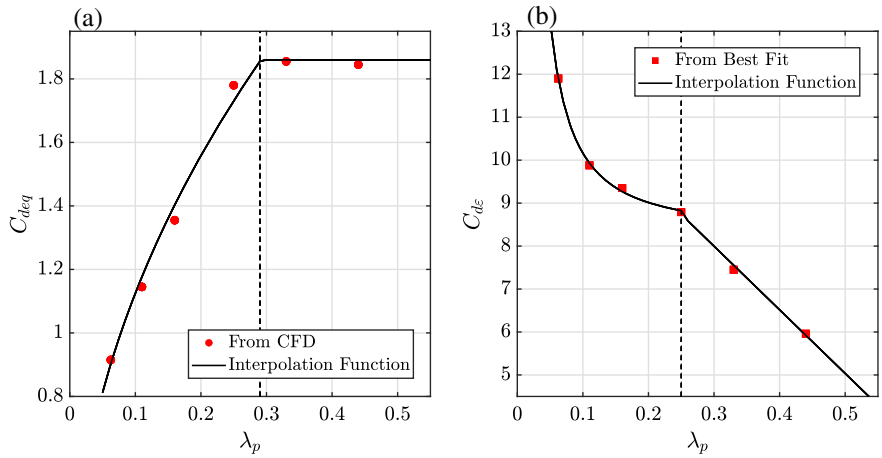

FIGURE 1 Variation of drag coefficients with λ_p, obtained with CFD simulations through Equation 14 for C_{deq} and through the best fit for $C_{d\varepsilon}$. [Colour figure can be viewed at wileyonlinelibrary.com]

TABLE 1 Overview of the different terms employed for the three UCPs tested against CFD output.

	k equation	ε equation	D_k	D_ε	Model constants
k–ℓ	Equation 5	Equation 6	Equation 9	—	C_d (Equation 14), $\ell_\varepsilon/C_\varepsilon$ (Equation 16)
k–ε–$T1$	Equation 5	Equation 7	Equation 9	Equation 10	C_d (Equation 14), $C_{d\varepsilon}$ (Equation 17)
k–ε–$T3$	Equation 5	Equation 7	Equation 11	Equation 12	C_d (Equation 14), $\alpha_2 = 8$, $\beta_2 = 5.5$

Finally, here we discuss the estimation of the terms for the k–ε–$3T$ model, the coefficients of which appear in Equations 11 and 12. Katul *et al.* (2004) showed that, for vegetated canopies, $\alpha_1 \sim \beta_1 \sim 1$, so we decided to keep these constants equal to 1 and to vary the two remaining coefficients in order to reduce the degrees of freedom. On the other hand, the comparison with the CFD output shows that the best results are obtained by setting $\alpha_2 = 8$ and $\beta_2 = 5.5$. The advantage of this method, with respect to k–ε–$1T$, relies on the lack of an additional drag coefficient dependent on λ_p for the dissipation rate equation.

2.3 | Turbulence closures

The 1-D column models (summarized in Table 1) evaluated in this work are as follows.

(1) The k–ℓ turbulence closure, where D_u and D_k are calculated through Equations 8 and 9, respectively. The drag coefficient C_d is estimated using the CFD simulations, and it is given by Equation 14. Moreover, the length scales are calculated with Equation 16. For further details, refer to Santiago and Martilli (2010).
2) The k–ε–$1T$ turbulence closure. Here D_u and D_k are the same as in the k–ℓ closure, but, in addition, the dissipation rate $\langle\overline{\varepsilon}\rangle$ is computed prognostically with Equation 22. The drag force induced by buildings specific for $\langle\overline{\varepsilon}\rangle$ (D_ε) is calculated through Equation 10, and the relative drag coefficient ($C_{d\varepsilon}$) is calculated with Equation 17. This estimate is deduced through a best-fit analysis between the k–ε model and the CFD output, for different values of λ_p.
3) The k–ε–$3T$ turbulence closure. D_u is the same as in the k–ℓ closure, but D_k is computed through Equation 11 and D_ε through Equation 12. The advantage with respect to the previous two models is that this scheme does not require a parameterization (i.e., a dependence between model parameters and λ_p) for either the length scale or the drag coefficient for the dissipation rate.

3 | SIMULATION SETUP

3.1 | CFD simulations

The CFD simulations used in this work were performed using the code FLUENT (ANSYS, 2016) and are based on the steady-state RANS equations and the standard k–ε turbulence closure. These simulations are identical to the ones also used in Santiago and Martilli (2010); for a detailed description of their setup, see Santiago *et al.* (2008).

Different packing densities of regularly staggered arrays of cubes, with incident wind along the x direction, are tested, at a three-dimensional resolution of 1 m. The urban geometry can be described by the plan area ratio (λ_p) and the front area ratio (λ_f):

$$\lambda_p = \frac{A_p}{A_t} = \frac{LW}{(W + S_y)(L + S_x)} \tag{18}$$

1477870x, 2023, 754, Downloaded from https://rmets.onlinelibrary.wiley.com/doi/10.1002/qj.4476 by Universita Di Trento, Wiley Online Library on [27/09/2023]. See the Terms and Conditions (https://onlinelibrary.wiley.com/terms-and-conditions) on Wiley Online Library for rules of use; OA articles are governed by the applicable Creative Commons License

and

$$\lambda_f = \frac{A_f}{A_t} = \frac{hW}{(W+S_y)(L+S_x)}, \tag{19}$$

where h is the building height, W and L are the building horizontal dimensions in the x and y directions, respectively, and S_x and S_y are the distances between the obstacles, as shown in Figure 2. In this study, the buildings are cubes with $h = W = L = 16$ m; therefore, for each urban configuration, $\lambda_p = \lambda_f$. In order to cover a large spectrum of possible urban geometries, as suggested by Grimmond and Oke (1999), six different packing densities are tested, with $\lambda_p = 0.0625, 0.11, 0.16, 0.25, 0.33, 0.44$. Assuming the dimensions of the buildings are kept constant, these values correspond to set $S_x = S_y = 48, 32, 24, 16, 12, 8$ m, respectively (see Figure 3 for a visual representation of the various packing densities). The extension of the domain is $4h$ in the vertical coordinate, while in the horizontal it depends on the packing density of the case study. Symmetric boundary conditions are set in the y direction and periodic boundary conditions in the direction of the wind (x), to simulate an infinite array of buildings. The flow is originated by a horizontal pressure gradient $\tau = \rho u_\tau^2/4h$, where $u_\tau = 1\,\mathrm{m\cdot s^{-1}}$ is the friction velocity. At the domain top, to obtain a purely horizontal parallel flow with null vertical motion, symmetric conditions are set, to obtain zero vertical derivatives for all the variables.

Simulation output for the case with $\lambda_p = 0.25$ was validated against DNS simulations (Coceal *et al.*, 2006) and experimental results (Cheng *et al.*, 2007) see also Santiago *et al.* (2008)).

3.2 | Simulations with the UCP

The UCP is run as a one-dimensional vertical column, with the same vertical resolution as the CFD simulations (i.e., 64 vertical layers with a resolution of 1 m). For the k–l closure, considering the equations for wind speed and TKE, starting from Equations 1 and 5, respectively, and neglecting the temporal derivative and the buoyancy production, since CFD simulations are performed in neutral conditions, the steady-state equations for wind speed and TKE are

$$0 = \frac{\partial}{\partial z}\left(\rho K_m \frac{\partial \langle \overline{u} \rangle}{\partial z}\right) - \rho D_u \tau, \tag{20}$$

$$0 = \frac{\partial}{\partial z}\left(\rho K_m \frac{\partial \langle \overline{k} \rangle}{\partial z}\right) + \rho K_m \left(\frac{\partial \langle \overline{u} \rangle}{\partial z}\right)^2 - \rho \langle \overline{\varepsilon} \rangle + \rho D_k, \tag{21}$$

where K_m is computed using Equation 3 and $\langle \overline{\varepsilon} \rangle$ using Equation 6.

For the k–ε closure, instead, K_m is computed through Equation 4, while $\langle \overline{\varepsilon} \rangle$ is calculated with its prognostic equation:

$$0 = \frac{\partial}{\partial z}\left(\rho \frac{K_m}{Pr} \frac{\partial \langle \overline{\varepsilon} \rangle}{\partial z}\right) + \rho c_1 \langle \overline{k} \rangle \left(\frac{\partial \langle \overline{u} \rangle}{\partial z}\right)^2 - \rho c_2 \frac{\langle \overline{\varepsilon} \rangle^2}{\langle \overline{k} \rangle} + \rho D_\varepsilon. \tag{22}$$

The expressions for calculating D_u, D_k, and D_ε are given in Section 2.1.

For the UCP, it is assumed that all horizontal gradients are null, except for a pressure gradient (τ) imposed to force a horizontal and parallel flow in the x direction, as in the CFD simulation. The goal is to use the single-column model to represent the whole array of cubes of the CFD domain. To compare the 3-D building-resolving CFD simulations with the 1-D simulations adopting the UCP, after the steady state is reached, the CFD outputs are averaged horizontally over each vertical level. Therefore, for any variable C, its spatial average is computed as

$$\langle C \rangle = \frac{1}{S_{air}} \iint C(x,y,t)\, dx\, dy, \tag{23}$$

where S_{air} is the surface occupied by air for each vertical level, excluding the surface occupied by buildings.

4 | RESULTS: VALIDATION OF ONE-DIMENSIONAL UCPS WITH SPATIALLY AVERAGED CFD SIMULATIONS

This section shows the results from the comparison between the three 1-D column models and the CFD simulations. To quantify the differences between the UCPs and the CFD simulations, taken as the reference, for each variable and value of λ_p tested the RMSE has been computed. It reads

$$RMSE = \sqrt{\frac{\sum_{n=1,N}\left(\langle \overline{\Psi_{CFD}} \rangle - \langle \overline{\Psi_{UCP}} \rangle\right)^2}{N}}, \tag{24}$$

where $\Psi = \left(u,\ k,\ \varepsilon,\ K_m,\ u'w'\right)$, and $n = 1, N$ are the vertical levels. Vertical profiles for the spatially averaged CFD (black dashed line), k–ℓ (red line), k–ε–$1T$ (blue line), and k–ε–$3T$ (green line) are shown for each λ_p for $\langle \overline{u} \rangle$, $\langle \overline{k} \rangle$, $\langle \overline{\varepsilon} \rangle$, K_m, $\langle \overline{u'w'} \rangle$ in Figures 4,5,6,7, and 8, respectively. All the variables, apart from $\langle \overline{\varepsilon} \rangle$, are normalized by means of u_τ and h. The RMSEs have been computed separately for the vertical points within the urban canopy

1477870x, 2023, 754, Downloaded from https://rmets.onlinelibrary.wiley.com/doi/10.1002/qj.4476 by Universita Di Trento, Wiley Online Library on [27/09/2023]. See the Terms and Conditions (https://onlinelibrary.wiley.com/terms-and-conditions) on Wiley Online Library for rules of use; OA articles are governed by the applicable Creative Commons License

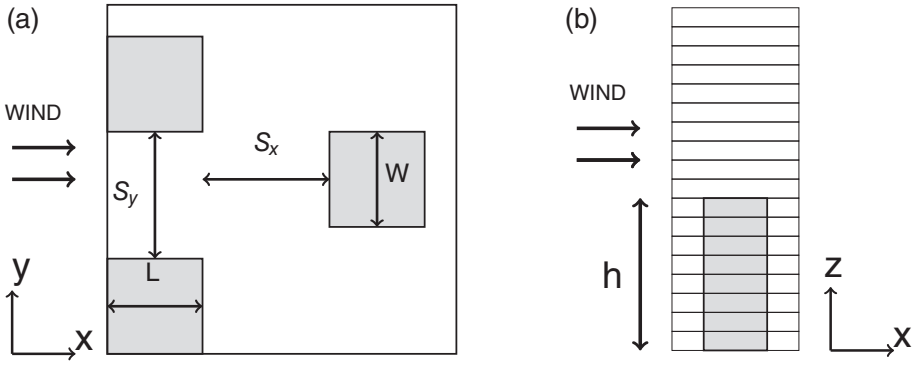

FIGURE 2 Design of the CFD simulations: (a) plan view of the staggered array, (b) vertical section for a single building.

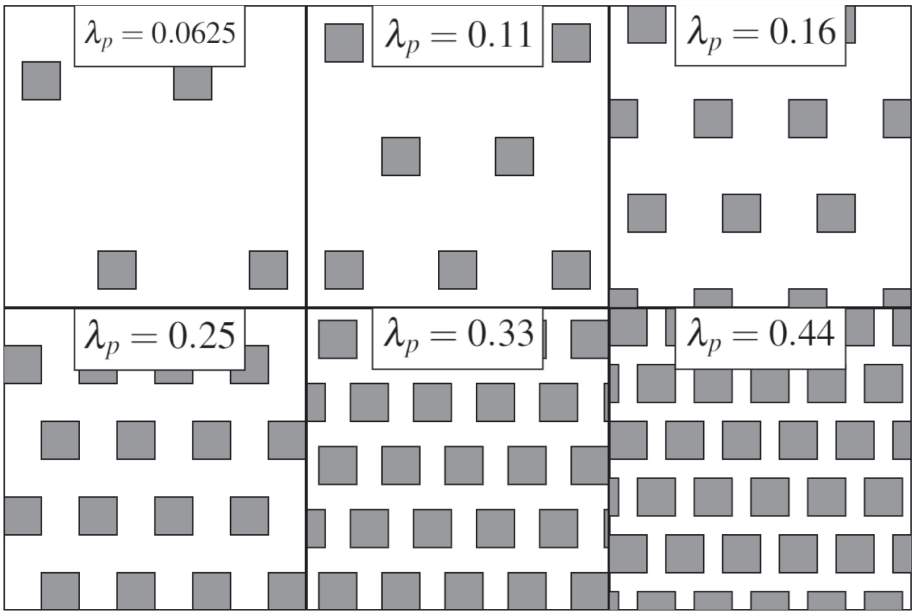

FIGURE 3 Plan view of the various packing densities tested in this study.

(Figure 9), above the urban canopy (Figure 10), and over the entire air column (Figure 11).

We will first discuss, for each variable considered, the results for the simulations with $\lambda_p = 0.25$, shown in panel (d) in the various figures, which is the case that was previously validated against experimental data and DNS simulations (Coceal *et al.*, 2006; Cheng *et al.*, 2007). Then, we will proceed to examine the vertical profile at varying λ_p.

4.1 | Wind speed

For $\lambda_p = 0.25$, the vertical profile of the spatially averaged wind speed (Figure 4d) resembles the typical profile of a neutral boundary layer with the presence of obstacles: up to $z \sim h/2$, the wind is almost constant for all UCP simulations, while the CFD simulation even displays negative wind speed, because it is able to resolve the vortexes developing within the urban canyons. At $z \sim h$ the largest wind shear occurs, because the horizontal pressure gradient forces a wind of $\sim 10\,\mathrm{m} \cdot \mathrm{s}^{-1}$ above the canopy, which is strongly reduced below roof level by the buildings. Indeed, over the canopy layer, the profile follows the typical log law. As expected, UCP simulations cannot capture the backward wind speed close to the surface, since in 1-D simulations buildings are not resolved explicitly and then recirculation cells cannot be reproduced. However, above $z \sim h/2$ all UCPs can reproduce the wind speed shown by the CFD simulation. In particular, k–ℓ is in good agreement up to the lower levels above the canopy, but from $z > 1.5h$ it underestimates the wind speed. On the other hand, k–ε–$3T$ works better than k–ℓ, but it slightly overestimates $\langle \overline{u} \rangle$ right above the building top, while k–ε–$1T$ is the UCP achieving the best agreement. For low λ_p, k–ℓ underestimates the wind speed within the canopy while overestimating it above the canopy. Instead, the two k–ε reproduce the wind speed within the canopy better (apart from a large underestimation in the layers closer to the ground). Moreover, they underestimate the wind speed above the canopy. In particular, k–ε–$3T$ shows the largest difference from the CFD simulations above the canopy. With increasing λ_p, all UCP simulations perform well in the upper part of the UCL ($h/2 < z < h$), while they cannot capture the recirculation cell at $z < h/2$. The maximum wind speed above roof level increases

1477870x, 2023, 754, Downloaded from https://rmets.onlinelibrary.wiley.com/doi/10.1002/qj.4476 by Universita Di Trento, Wiley Online Library on [27/09/2023]. See the Terms and Conditions (https://onlinelibrary.wiley.com/terms-and-conditions) on Wiley Online Library for rules of use; OA articles are governed by the applicable Creative Commons License

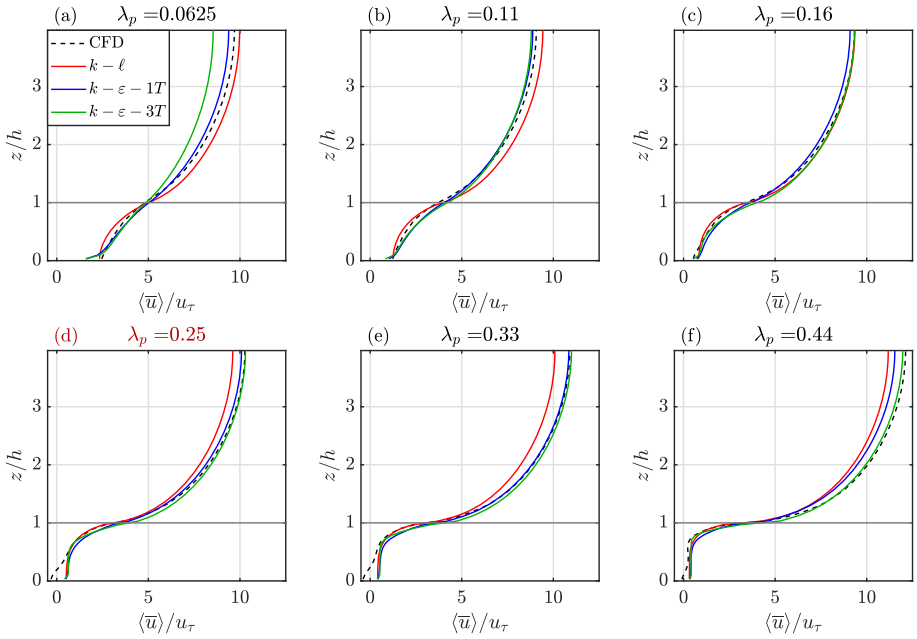

FIGURE 4 Vertical profiles of normalized mean wind speed for all the values of λ_p tested. Panel (d) refers to the packing density, the CFD of which has been validated against experimental data. [Colour figure can be viewed at wileyonlinelibrary.com]

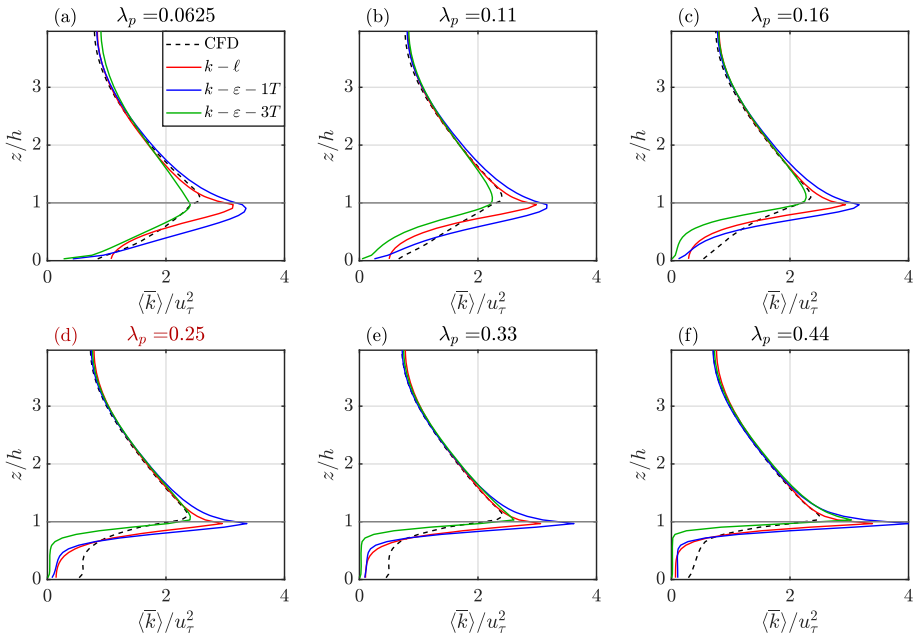

FIGURE 5 Vertical profiles of normalized mean TKE for all the values of λ_p tested. Panel (d) refers to the packing density, the CFD of which has been validated against experimental data. [Colour figure can be viewed at wileyonlinelibrary.com]

with increasing λ_p, since packed buildings produce less turbulence through the drag, and therefore less energy is dissipated at higher levels. Above the canopy layer, the largest discrepancies are found for k–ℓ, which overestimates the maximum wind speed for low λ_p values and underestimates it for higher λ_p. Instead, the two k–ϵ capture the wind maximum better, with the best agreement shown by k–ε–$1T$ at low λ_p and by k–ε–$3T$ at high λ_p.

4.2 | Turbulent kinetic energy

Since the largest shear occurs near the building top, the TKE vertical profile exhibits maxima around h, as shown in Figure 5. For $\lambda_p = 0.25$, within the canopy layer the TKE is low and almost constant with height. Then it grows rapidly close to the building top and finally decreases with increasing height above roof level. All UCPs tend to underestimate the TKE within the canopy layer, since they underestimate the wind shear. On the other hand, they can reproduce the peak well at $z \sim h$. Specifically, both k–ℓ and k–ε–$1T$ overestimate the intensity of the peak and underestimate its height. On the other hand, k–ε–$3T$ is the best in reproducing the TKE peak, despite the higher underestimation within the canopy layer. Above the canopy, all simulations can represent the decrease of TKE with good accuracy.

Within the canopy, UCPs perform better for low values of λ_p than for high values, where TKE decreases too fast

1477870x, 2023, 754, Downloaded from https://rmets.onlinelibrary.wiley.com/doi/10.1002/qj.4476 by Universita Di Trento, Wiley Online Library on [27/09/2023]. See the Terms and Conditions (https://onlinelibrary.wiley.com/terms-and-conditions) on Wiley Online Library for rules of use; OA articles are governed by the applicable Creative Commons License

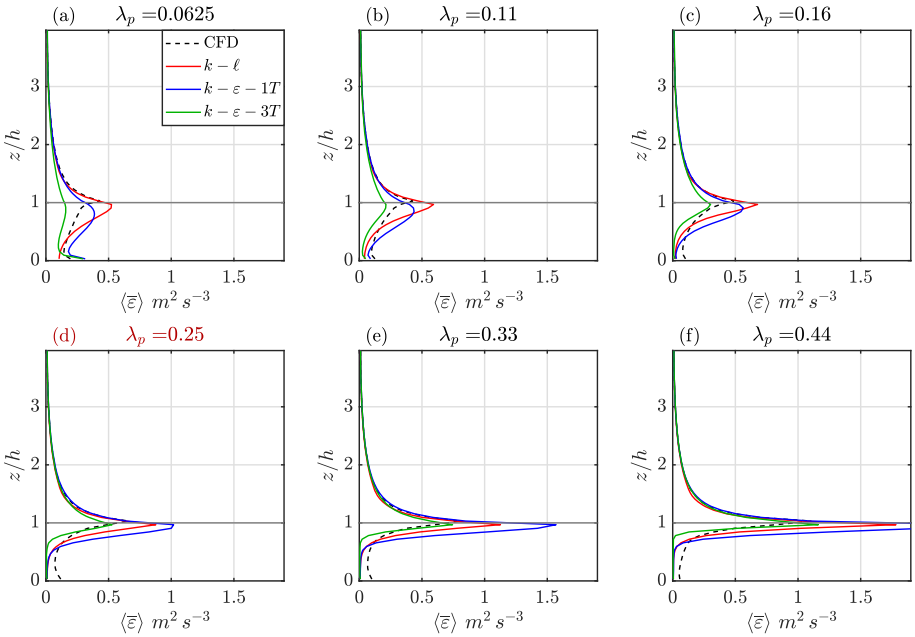

FIGURE 6 Vertical profiles of mean dissipation rate for all the values of λ_p tested. Panel (d) refers to the packing density, the CFD of which has been validated against experimental data. [Colour figure can be viewed at wileyonlinelibrary.com]

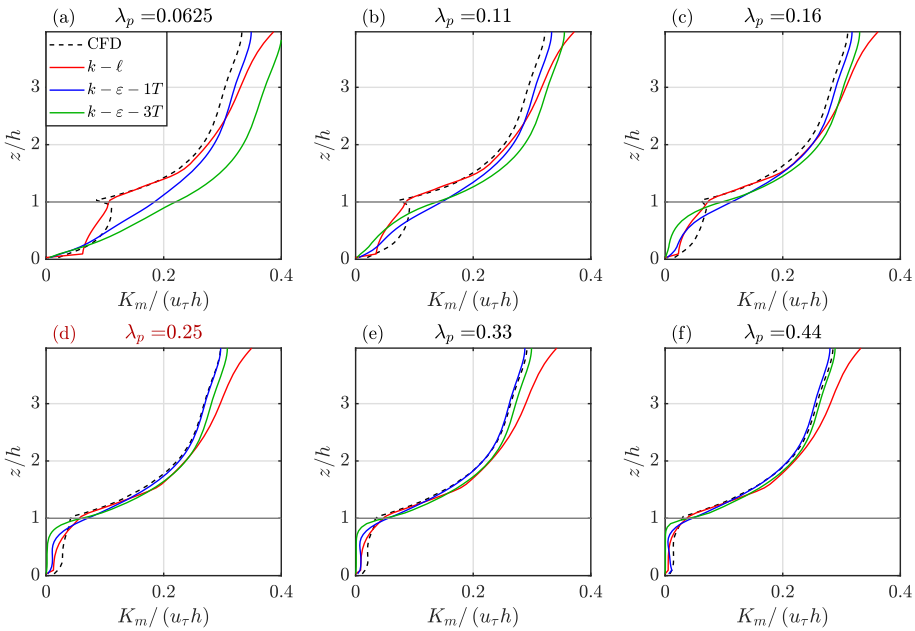

FIGURE 7 Vertical profiles of normalized mean eddy diffusivity for all the values of λ_p tested. Panel (d) refers to the packing density, the CFD of which has been validated against experimental data. [Colour figure can be viewed at wileyonlinelibrary.com]

compared with CFD simulations. The TKE peak at $z \sim h$ presents similar values with varying λ_p. While k–ℓ and k–ε–$1T$ generally overestimate the peak for all values of λ_p, k–ε–$3T$ is in better agreement with CFD simulations, despite a slight underestimation for low λ_p. Finally, above the canopy layer, all UCPs reproduce the vertical profile of TKE well for all the cases tested.

4.3 | Dissipation rate

The vertical profiles of dissipation rate shown in Figure 6 display a shape similar to those of the TKE, with the highest value at $z \sim h$. Again, for $\lambda_p = 0.25$, k–ℓ and k–ε–$1T$ overestimate the peak intensity, while k–ε–$3T$ agrees better with the CFD simulations. On the other hand, all UCP simulations underestimate $\langle\overline{\varepsilon}\rangle$ for $z < h/2$, while they can capture the decrease of $\langle\overline{\varepsilon}\rangle$ above roof level. While the TKE peak remains approximately constant with increasing λ_p, the dissipation-rate peak largely increases with λ_p. The behavior of the different UCPs is similar to that found for the TKE: within the canopy, UCPs agree better with CFD data at low λ_p values than at high values. In general, for $h/2 < z < h$, k–ℓ and k–ε–$1T$ overestimate the dissipation rate. The best results are displayed by k–ε–$3T$: despite an underestimation for low λ_p values, it can capture the increase of $\langle\overline{\varepsilon}\rangle$ approaching $z = h$ and reproduces the peak well. Instead, the other two

1477870x, 2023, 754, Downloaded from https://rmets.onlinelibrary.wiley.com/doi/10.1002/qj.4476 by Universita Di Trento, Wiley Online Library on [27/09/2023]. See the Terms and Conditions (https://onlinelibrary.wiley.com/terms-and-conditions) on Wiley Online Library for rules of use; OA articles are governed by the applicable Creative Commons License

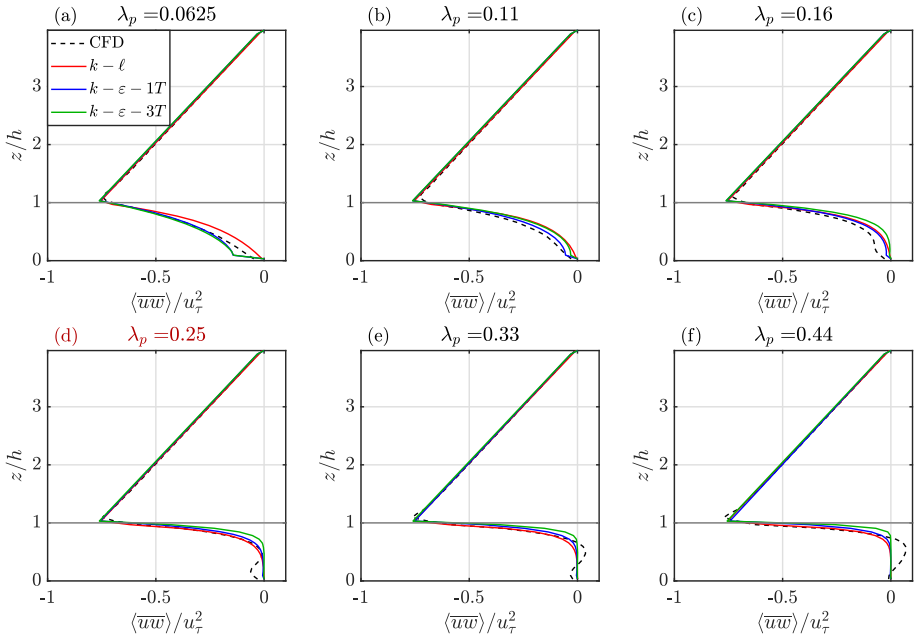

FIGURE 8 Vertical profiles of normalized mean vertical momentum flux for all the values of λ_p tested. Panel (d) refers to the packing density, the CFD of which has been validated against experimental data. [Colour figure can be viewed at wileyonlinelibrary.com]

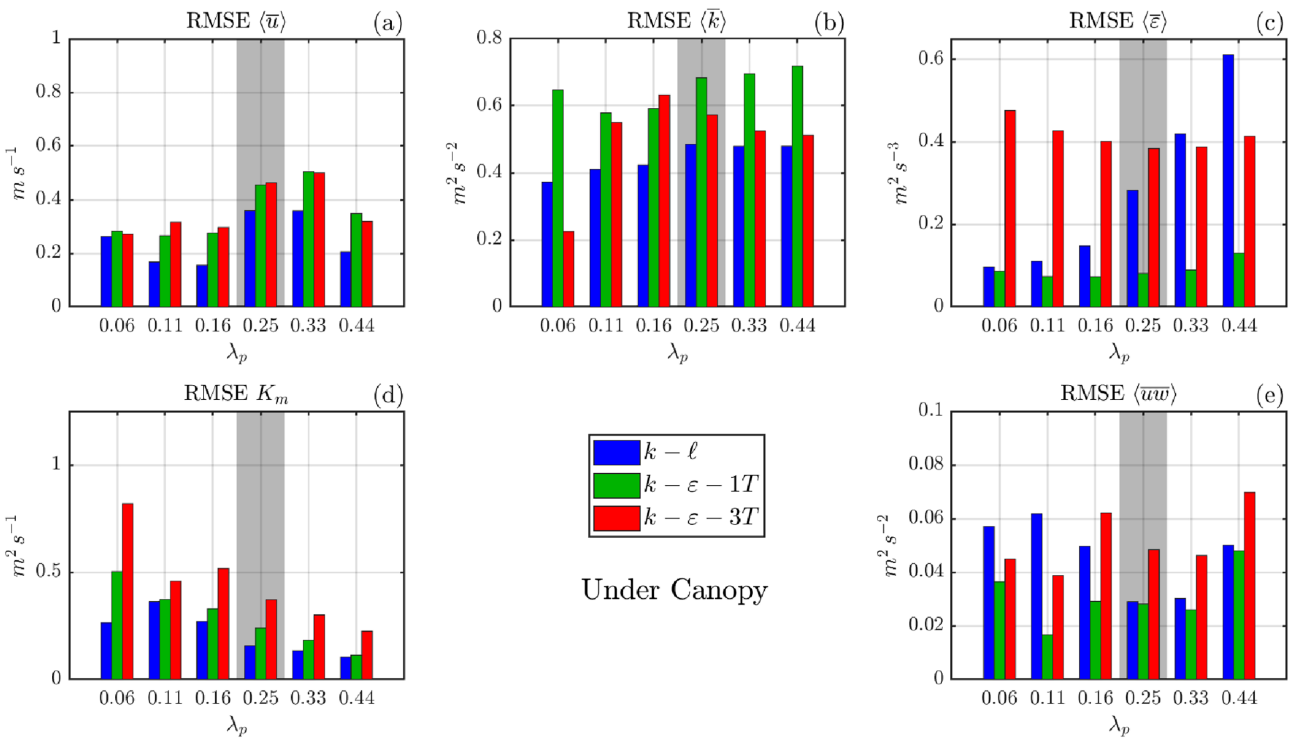

FIGURE 9 RMSEs computed for the vertical points within the UCL ($0 < z \leq h$), for all the variables and λ_p values. The shaded area highlights the packing density validated against experimental data. [Colour figure can be viewed at wileyonlinelibrary.com]

parameterizations tend to overestimate the maximum, especially for high λ_p values.

4.4 | Eddy diffusivity

Eddy diffusivity can be derived through Equations 3 and 4 for k–ℓ and k–ε, respectively. Values are shown in Figure 7. Vertical profiles of eddy diffusivity follow an almost linear increase ($K_m \propto u_\star z$ for the Monin–Obukhov similarity theory) above $z \sim 2h$. Below this level, K_m increases slowly up to $z \sim h$, and then more rapidly up to $z \sim 2h$. Because of the underestimation of the TKE, for $\lambda = 0.25$ all the UCPs underestimate K_m within the canopy layer. Around $z \sim h$, instead, they all start to agree with the CFD simulations, with a better agreement for k–ℓ and k–ε–$3T$, which

1477870x, 2023, 754, Downloaded from https://rmets.onlinelibrary.wiley.com/doi/10.1002/qj.4476 by Universita Di Trento, Wiley Online Library on [27/09/2023]. See the Terms and Conditions (https://onlinelibrary.wiley.com/terms-and-conditions) on Wiley Online Library for rules of use; OA articles are governed by the applicable Creative Commons License

capture the height and the slope of maximum increase of the eddy diffusivity better. From $z \sim 2h$, k–ℓ eddy diffusivity starts to diverge, with an overestimation of K_m, while the two k–ε are in better agreement with the CFD simulations. This is an expected result, since the two k–ε and the CFD simulations adopt the same turbulence closure, which, at higher levels in the absence of obstacles and therefore in the case of horizontal homogeneity, becomes identical.

The major difference between different λ_p takes place within the canopy layer, where K_m decreases with increasing λ_p. The largest discrepancies between CFD and UCP simulations occur for low λ_p values, where k–ε–$1T$ and k–ε–$3T$ tend to overestimate the eddy diffusivity, especially for $0 < z < 2h$. Increasing λ_p, all UCPs tend to reproduce K_m well up to $z \sim 2h$. Instead, above this height, k–ℓ overestimates the eddy diffusivity. This overestimation explains the underestimation of the wind speed above the canopy layer shown in Figure 4d–f: the higher the eddy diffusivity, the lower the wind speed, since the vertical diffusion is enhanced.

4.5 | Momentum flux

Concerning the spatially averaged vertical momentum flux (Figure 8), within the canopy for $\lambda_p = 0.25$ the profile is constant (and almost null) for all the UCPs, while the CFD simulation shows small oscillation anomalies because of the recirculation cells. A negative peak is found at $z \sim h$, which is captured well by all the UCPs, as well as the vertical profile above the canopy layer.

Within the canopy layer, $\langle \overline{u'w'} \rangle$ increases in absolute value up to $z \sim h$ for all the cases tested, with a slope that is quasilinear for low λ_p values. On the other hand, for higher λ_p, $\langle \overline{u'w'} \rangle$ is almost null in the lower part of the canopy layer and then increases rapidly (in absolute value) approaching the canopy layer top. The negative peak at $z \sim h$ presents the same value for all the configurations. Above the canopy, the momentum flux decreases linearly (in absolute value) with the same rate, and similarly for all λ_p. Within the canopy, the two k–ε outperform k–ℓ for low λ_p values, while, at higher λ_p, k–ε–$3T$ overestimates the height at which the turbulent momentum flux is almost null. Above the canopy, all the UCPs display similar behaviors, correctly capturing the linear trend.

4.6 | Root-mean-square errors

Figures 9,10, and 11 show the RMSEs calculated between the CFD simulations and the three UCPs for all the λ_p values, respectively under the canopy, above the canopy, and along all the air column. In general, the errors above

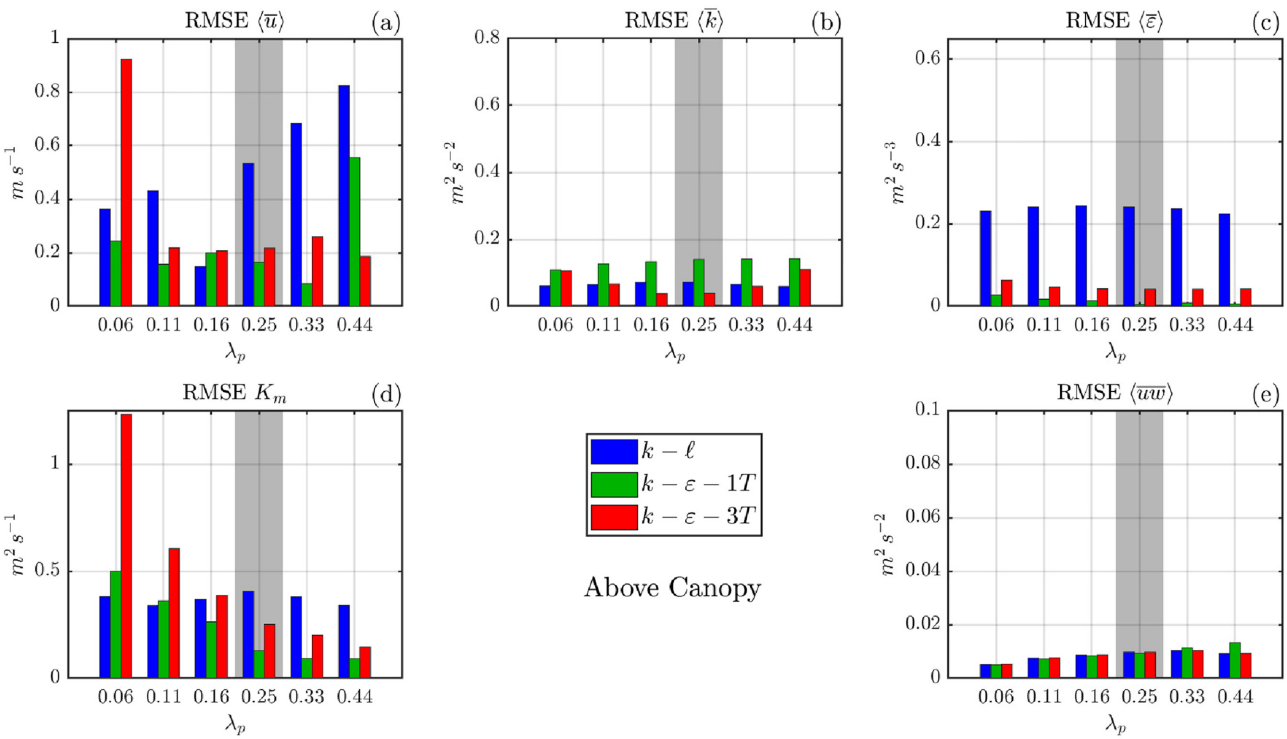

FIGURE 10 RMSEs computed for the vertical points above the UCL ($h < z < 4h$), for all the variables and λ_p values. The shaded area highlights the packing density validated against experimental data. [Colour figure can be viewed at wileyonlinelibrary.com]

1477870x, 2023, 754, Downloaded from https://rmets.onlinelibrary.wiley.com/doi/10.1002/qj.4476 by Universita Di Trento, Wiley Online Library on [27/09/2023]. See the Terms and Conditions (https://onlinelibrary.wiley.com/terms-and-conditions) on Wiley Online Library for rules of use; OA articles are governed by the applicable Creative Commons License

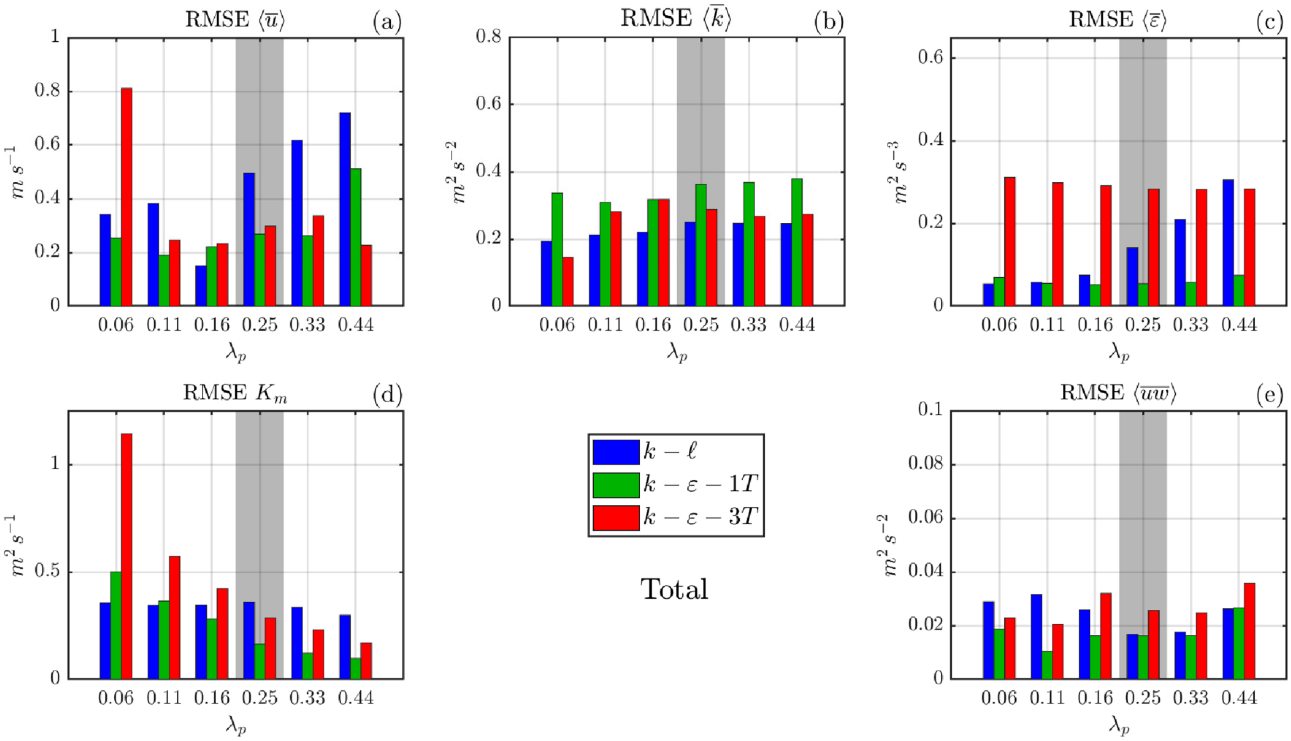

FIGURE 11 RMSEs computed for all the vertical points in the column of air ($0 < z < 4h$), for all the variables and λ_p values. The shaded area highlights the packing density validated against experimental data. [Colour figure can be viewed at wileyonlinelibrary.com]

the canopy are half as large as those within the canopy, since the mean flow is disturbed by buildings, and the UCP simulations cannot resolve the obstacles.

Wind speed RMSEs (Figures 9a, 10a, and 11a) are similar for all the UCPs within the canopy layer, with a slightly better performance by k–ℓ. However, above the canopy layer, k–ℓ departs from CFD simulations with increasing λ_p. On the other hand, the error displayed by the two k–ε schemes remains low and constant for the central range of λ_p, with higher discrepancies at the two extremes.

Regarding the TKE, errors within the canopy are lower for k–ℓ, followed by k–ε–$3T$ (Figure 9b) and almost constant with λ_p for all UCPs. Above the canopy, instead, k–ε–$3T$ performs better than the other two. Analyzing the RMSEs of the dissipation rate within the canopy (Figure 9c), while k–ℓ shows increasing errors with λ_p, k–ε–$1T$ maintains constant and very low errors, while k–ε–$3T$ displays RMSEs that increase with λ_p. Above the canopy, instead, both k–ε outperform k–ℓ, with the best performance shown by k–ε–$1T$.

Errors in the eddy diffusivity are similar for all the UCPs under the canopy (Figure 9d), with slightly worse results for k–ε–$3T$. However, errors decrease substantially at increasing λ_p. Above the canopy, instead, while both k–ε increase their performance with increasing λ_p, k–ℓ maintains the same error, underperforming for high λ_p values.

The errors of $\langle\overline{u'w'}\rangle$ are similar for all the UCPs under the canopy, with slightly better results for k–ε–$1T$, whereas above the canopy the errors are comparable for all the UCPs. Considering the whole air column (Figure 11), for $\lambda_p = 0.25$ the two k–ε perform better than k–ℓ in terms of wind speed, eddy diffusivity, and especially dissipation rate. Errors are similar for all the UCPs for the TKE and vertical momentum flux, with slightly better results shown by k–ε–$1T$ for the latter.

5 | DISCUSSION AND CONCLUSIONS

In this work, we propose a one-dimensional urban canopy scheme, based on the k–ϵ turbulence closure, suitable for reproducing the wind flow within the urban canopy layer. CFD simulations with a spatial resolution high enough to resolve buildings and their interaction with the airflow were assumed as a reference benchmark. The CFD simulations from Santiago and Martilli (2010), performed for idealized urban configurations (staggered arrays of cubes), have been used first to derive suitable parameterizations of the drag coefficients and then to evaluate the UCP schemes through a spatial average over the simulation domain.

One-dimensional k–ε turbulence closures had already been successfully employed for reproducing the flow

1477870x, 2023, 754, Downloaded from https://rmets.onlinelibrary.wiley.com/doi/10.1002/qj.4476 by Universita Di Trento, Wiley Online Library on [27/09/2023]. See the Terms and Conditions (https://onlinelibrary.wiley.com/terms-and-conditions) on Wiley Online Library for rules of use; OA articles are governed by the applicable Creative Commons License

within vegetated canopies (see, e.g., Katul *et al.* (2004)), but never for urban environments. Here, we propose two different versions of the k–ε closure, starting from previously developed UCPs based on the k–ℓ turbulence scheme. The simplest one adopts an additional source term for the prognostic $\langle\bar{\varepsilon}\rangle$ equation (k–ε–1T), the drag coefficient of which, depending on the plan area ratio, has been derived from the CFD building-resolving simulations. The second one includes an additional term for the prognostic TKE equation and two additional terms for the prognostic equation for the dissipation rate (k–ε–3T). The advantage of the latter is that it does not need the parameterization of the drag coefficient for the dissipation rate equation, nor a model for the turbulent length scale (as Santiago and Martilli (2010) did for the k–ℓ closure), so it depends on the CFD only for the computation of the additional terms in the equation due to the presence of buildings.

The results of the comparison between one-dimensional UCPs and CFD outputs demonstrate that the new closures represent the vertical profiles of the relevant variables reasonably, capturing the vertical heterogeneity of the flow induced by the building's array. The sensitivity to λ_p values is captured well by all the UCPs, since vertical gradients of both mean and turbulent variables increase with increasing λ_p. Comparing the various UCPs, the two k–ε enhance the reproduction of wind speed with respect to k–ℓ, especially far from the UCL. In particular, k–ε–1T works better for low values of λ_p and k–ε–3T for higher values. k–ε–1T improves the reproduction of the dissipation rate and eddy diffusivity, especially at high λ_p values. On the other hand, k–ℓ is the best-performing closure in reproducing the vertical momentum flux, while, considering the whole air column, no significant differences are found between the UCPs for the TKE.

Besides the improvement in reproducing the flow, the newly developed k–ε closures rely less than the k–ℓ scheme on the CFD output for the derivation of the drag coefficients, since ad hoc turbulence length scales and displacement heights are not required. In particular, k–ε–1T needs two drag coefficients, while k–ε–3T is even less dependent on the CFD results, since it uses a single drag coefficient, which still depends on λ_p, but it is the only parameter added to the traditional k–ε closure and is the same derived in Santiago and Martilli (2010).

Based on the results presented in this work, the formulation proposed here can be incorporated within mesoscale models, aiming to improve the representation of the interaction between cities and the atmospheric boundary layer for real case studies. Moreover, using a k–ε-based turbulence closure may be beneficial in terms of the coupling between meso- and microscale models, since usually microscale simulations are performed with similar closure schemes, and turbulent variables can be passed as input, resulting in a more robust coupling. In the current state, the new model is limited to staggered arrays of buildings with the same height, and the drag coefficients C_d and $C_{d\varepsilon}$ are still independent of the height from the ground. Future studies will include the comparison of the current scheme with recently developed high-resolution LES for the same idealized case study (Nazarian *et al.* (2020)), as well as its implementation within more complex state-of-the-art UCPs like BEP (Martilli *et al.*, 2002), which also includes thermal exchanges between urban structures and the atmosphere.

AUTHOR CONTRIBUTIONS

Andrea Zonato: conceptualization; dataCuration; formalAnalysis; investigation; methodology; software; validation; writingOriginalDraft; writingReviewEditing. **Alberto Martilli:** conceptualization; methodology; supervision; writing – review and editing. **Jose Luis Santiago:** data curation; software; writing – review and editing. **Dino Zardi:** project administration; resources; supervision; writing – review and editing. **Lorenzo Giovannini:** conceptualization; methodology; supervision; writing – original draft; writing – review and editing.

ORCID

Andrea Zonato https://orcid.org/0000-0002-9174-1618
Lorenzo Giovannini https://orcid.org/0000-0003-1650-0344

REFERENCES

Ahmad Zaki, S., Hagishima, A. and Tanimoto, J. (2012) Experimental study of wind-induced ventilation in urban building of cube arrays with various layouts. *Journal of Wind Engineering and Industrial Aerodynamics*, 103, 31–40. https://doi.org/10.1016/j.jweia.2012.02.008.

ANSYS. (2016) Ansys fluent–cfd software | ansys. http://www.ansys.com/products/fluids/ansys-fluent.

Antoniou, N., Montazeri, H., Wigo, H., Neophytou, M.K., Blocken, B. and Sandberg, M. (2017) CFD and wind-tunnel analysis of outdoor ventilation in a real compact heterogeneous urban area: Evaluation using "air delay". *Building and Environment*, 126, 355–372.

Auvinen, M., Boi, S., Hellsten, A., Tanhuanpää, T. and Järvi, L. (2020) Study of realistic urban boundary layer turbulence with high-resolution large-eddy simulation. *Atmosphere*, 11, 201. https://www.mdpi.com/2073-4433/11/2/201.

Beljaars, A.C.M., Walmsley, J.L. and Taylor, P.A. (1987) A mixed spectral finite-difference model for neutrally stratified boundary-layer flow over roughness changes and topography. *Boundary-Layer Meteorology*, 38, 273–303. http://link.springer.com/10.1007/BF00122448.

Bougeault, P. and Lacarrere, P. (1989) Parameterization of orography-induced turbulence in a mesobeta–scale model. *Monthly Weather Review*, 117, 1872–1890. http://journals.

1477870x, 2023, 754, Downloaded from https://rmets.onlinelibrary.wiley.com/doi/10.1002/qj.4476 by Universita Di Trento, Wiley Online Library on [27/09/2023]. See the Terms and Conditions (https://onlinelibrary.wiley.com/terms-and-conditions) on Wiley Online Library for rules of use; OA articles are governed by the applicable Creative Commons License

ametsoc.org/doi/10.1175/1520-0493(1989)117%3C1872:POOITI%3E2.0.CO;2.

Chen, L., Hang, J., Sandberg, M., Claesson, L., Di Sabatino, S. and Wigo, H. (2017) The impacts of building height variations and building packing densities on flow adjustment and city breathability in idealized urban models. *Building and Environment*, 118, 344–361. doi:10.1016/j.buildenv.2017.03.042. https://linkinghub.elsevier.com/retrieve/pii/S0360132317301518

Cheng, H., Hayden, P., Robins, A. and Castro, I. (2007) Flow over cube arrays of different packing densities. *Journal of Wind Engineering and Industrial Aerodynamics*, 95, 715–740. https://linkinghub.elsevier.com/retrieve/pii/S016761050700013X.

Coceal, O. and Belcher, S.E. (2004) A canopy model of mean winds through urban areas. *Quarterly Journal of the Royal Meteorological Society*, 130, 1349–1372.

Coceal, O., Thomas, T.G., Castro, I.P. and Belcher, S.E. (2006) Mean flow and turbulence statistics over groups of urban-like cubical obstacles. *Boundary-Layer Meteorology*, 121, 491–519. http://link.springer.com/10.1007/s10546-006-9076-2.

Dai, Y., Mak, C.M., Ai, Z. and Hang, J. (2018) Evaluation of computational and physical parameters influencing CFD simulations of pollutant dispersion in building arrays. *Building and Environment*, 137, 90–107. doi:10.1016/j.buildenv.2018.04.005. https://linkinghub.elsevier.com/retrieve/pii/S0360132318302099

Di Sabatino, S., Solazzo, E., Paradisi, P. and Britter, R. (2008) A simple model for spatially-averaged wind profiles within and above an urban canopy. *Boundary-Layer Meteorology*, 127, 131–151. http://link.springer.com/10.1007/s10546-007-9250-1.

Duynkerke, P.G. (1988) Application of the E–ϵ turbulence closure model to the neutral and stable atmospheric boundary layer.

Giometto, M., Christen, A., Egli, P., Schmid, M., Tooke, R., Coops, N. and Parlange, M. (2017) Effects of trees on mean wind, turbulence and momentum exchange within and above a real urban environment. *Advances in Water Resources*, 106, 154–168. doi:10.1016/j.advwatres.2017.06.018. https://linkinghub.elsevier.com/retrieve/pii/S0309170817306486

Giovannini, L., Zardi, D. and de Franceschi, M. (2013) Characterization of the thermal structure inside an urban canyon: field measurements and validation of a simple model. *Journal of Applied Meteorology and Climatology*, 52, 64–81. http://journals.ametsoc.org/doi/abs/10.1175/JAMC-D-12-06.1.

Grimmond, C.S.B. and Oke, T.R. (1999) Aerodynamic properties of urban areas derived from analysis of surface form. *Journal of Applied Meteorology*, 38, 1262–1292. http://journals.ametsoc.org/doi/abs/10.1175/1520-0450%281999%29038%3C1262%3AAPOUAD%3E2.0.CO%3B2.

Kanda, M., Kawai, T., Kanega, M., Moriwaki, R., Narita, K. and Hagishima, A. (2005) A simple energy balance model for regular building arrays. *Boundary-Layer Meteorology*, 116, 423–443. http://link.springer.com/10.1007/s10546-004-7956-x.

Katul, G.G., Mahrt, L., Poggi, D. and Sanz, C. (2004) One- and two-equation models for canopy turbulence. *Boundary-Layer Meteorology*, 113, 81–109. http://link.springer.com/10.1023/B:BOUN.0000037333.48760.e5.

Kusaka, H., Kondo, H., Kikegawa, Y. and Kimura, F. (2001) A simple single-layer urban canopy model for atmospheric models: Comparison with multi-layer and slab models. *Boundary-Layer Meteorol.*, 101, 329–358. https://doi.org/10.1023/A:1019207923078.

Langland, R.H. and Liou, C.-S. (1996) Implementation of an E –ϵ parameterization of vertical subgrid-scale mixing in a regional model. *Monthly Weather Review*, 124, 905–918. http://journals.ametsoc.org/doi/10.1175/1520-0493(1996)124%3C0905:IOAPOV%3E2.0.CO;2.

Launder, B. and Spalding, D. (1974) The numerical computation of turbulent flows. *Computer Methods in Applied Mechanics and Engineering*, 3, 269–289.

Launder, B. and Spalding, D. (1983) The numerical computation of turbulent flows. In: *Numerical prediction of flow, heat transfer, turbulence and combustion*. Pergamon: Elsevier. pp. 96–116. https://linkinghub.elsevier.com/retrieve/pii/B9780080309378500167.

Liu, J., Chen, J.M., Black, T.A. and Novak, M.D. (1996) E–ϵ modelling of turbulent air flow downwind of a model forest edge. *Boundary-Layer Meteorology*, 77, 21–44.

Martilli, A., Clappier, A. and Rotach, M.W. (2002) An urban surface exchange parametrization for mesoscale models. *Boundary-Layer Meteorology*, 104, 261–304.

Masson, V. (2000) A physically-based scheme for the urban energy budget in atmospheric models. *Boundary-Layer Meteorology*, 94, 357–397. http://link.springer.com/10.1023/A:1002463829265.

Masson, V. and Seity, Y. (2009) Including atmospheric layers in vegetation and urban offline surface schemes. *Journal of Applied Meteorology and Climatology*, 48, 1377–1397. http://journals.ametsoc.org/doi/10.1175/2009JAMC1866.1.

Nazarian, N., Krayenhoff, E.S. and Martilli, A. (2020) A one-dimensional model of turbulent flow through "urban" canopies (MLUCM v2.0): updates based on large-eddy simulation. *Geoscientific Model Development*, 13(3), 937–953. https://doi.org/10.5194/gmd-13-937-2020.

Poggi, D., Porporato, A., Ridolfi, L., Albertson, J.D. and Katul, G.G. (2004) The effect of vegetation density on canopy sub-layer turbulence. *Boundary-Layer Meteorology*, 111, 565–587. http://link.springer.com/10.1023/B:BOUN.0000016576.05621.73.

Roth, M. (2000) Review of atmospheric turbulence over cities. *Quarterly Journal of the Royal Meteorological Society*, 126, 941–990. http://www.ingentaselect.com/rpsv/cgi-bin/cgi?ini=xref&body=linker&reqdoi=10.1256/smsqj.56408.

Santiago, J.L., Coceal, O., Martilli, A. and Belcher, S.E. (2008) Variation of the sectional drag coefficient of a group of buildings with packing density. *Boundary-Layer Meteorology*, 128, 445–457.

Santiago, J.L. and Martilli, A. (2010) A dynamic urban canopy parameterization for mesoscale models based on computational fluid dynamics Reynolds-averaged Navier-Stokes microscale simulations. *Boundary-Layer Meteorology*, 137, 417–439.

Sanz, C. (2003) A note on κ–ϵ modelling of vegetation canopy air-flows. *Boundary-Layer Meteorology*, 108, 191–197.

Tolladay, J. and Chemel, C. (2021) Numerical modelling of neutral boundary-layer flow across a forested ridge. *Boundary-Layer Meteorology*, 180, 457–476. https://doi.org/10.1007/s10546-021-00628-y.

Uno, I., Ueda, H. and Wakamatsu, S. (1989) Numerical modeling of the nocturnal urban boundary layer. *Boundary-Layer Meteorology*, 49, 77–98. http://link.springer.com/10.1007/BF00116406.

van der Laan, M.P., Kelly, M.C. and Sørensen, N.N. (2017) A new k-epsilon model consistent with Monin-Obukhov similarity theory. *Wind Energy*, 20, 479–489. http://doi.wiley.com/10.1002/we.2017.

Wilson, J.D., Finnigan, J.J. and Raupach, M.R. (1998) A first-order closure for disturbed plant-canopy flows, and its application to winds in a canopy on a ridge. *Quarterly Journal of the Royal*

1477870x, 2023, 754, Downloaded from https://rmets.onlinelibrary.wiley.com/doi/10.1002/qj.4476 by Universita Di Trento, Wiley Online Library on [27/09/2023]. See the Terms and Conditions (https://onlinelibrary.wiley.com/terms-and-conditions) on Wiley Online Library for rules of use; OA articles are governed by the applicable Creative Commons License

Meteorological Society, 124, 705–732. http://www.ingentaselect.com/rpsv/cgi-bin/cgi?ini=xref&body=linker&reqdoi=10.1256/smsqj.54703.

Zeng, X., Wang, Y. and MacCall, B.T. (2020) A k–ϵ turbulence model for the stable atmosphere. *Journal of the Atmospheric Sciences*, 77, 167–184. http://journals.ametsoc.org/doi/10.1175/JAS-D-19-0085.1.

Zhang, C., Wang, Y. and Xue, M. (2020) Evaluation of an E-ϵ and three other boundary layer parameterization schemes in the WRF model over the southeast pacific and the Southern Great Plains. *Monthly Weather Review*, 148, 1121–1145.

Zonato, A., Martilli, A., Jimenez, P.A., Dudhia, J., Zardi, D. and Giovannini, L. (2022) A new k–ϵ turbulence parameterization for mesoscale meteorological models. *Monthly Weather Review*, 150, 2157–2174. https://journals.ametsoc.org/view/journals/mwre/150/8/MWR-D-21-0299.1.xml.

How to cite this article: Zonato, A., Martilli, A., Santiago, J.L., Zardi, D. & Giovannini, L. (2023) On a new one-dimensional ***k–ε*** turbulence closure for building-induced drag. *Quarterly Journal of the Royal Meteorological Society*, 149(754), 1674–1689. Available from: https://doi.org/10.1002/qj.4476

1477870x, 2023, 754, Downloaded from https://rmets.onlinelibrary.wiley.com/doi/10.1002/qj.4476 by Universita Di Trento, Wiley Online Library on [27/09/2023]. See the Terms and Conditions (https://onlinelibrary.wiley.com/terms-and-conditions) on Wiley Online Library for rules of use; OA articles are governed by the applicable Creative Commons License